



## Article

# Combining Area-Based and Individual Tree Metrics for Improving Merchantable and Non-Merchantable Wood Volume Estimates in Coastal Douglas-Fir Forests

Jason Kelley <sup>1,\*</sup> , J. A. (Tony) Trofymow <sup>2,3</sup> and Christopher Bone <sup>1</sup><sup>1</sup> Department of Geography, University of Victoria, Victoria, BC V8P 5C2, Canada; chrisbone@uvic.ca<sup>2</sup> Natural Resources Canada, Canadian Forest Service, Pacific Forestry Centre, 506 West Burnside Road, Victoria, BC V8Z 1M5, Canada; tony.trofymow@canada.ca<sup>3</sup> Department of Biology, University of Victoria, Victoria, BC V8P 5C2, Canada

\* Correspondence: jkelley@uvic.ca

**Abstract:** Forest management practices can increase climate change mitigation potential through applications focused on carbon budgets. One such application involves utilizing non-merchantable material (i.e., logging residues typically piled and burned) for bio-energy. However, limited remote sensing data is available for estimating wood residues until after timber has been harvested, at which point recovery of residual wood is of little financial interest. This research utilizes a hybrid method to develop models that provide pre-harvest estimates of the amount of merchantable and non-merchantable material that would result from harvesting and investigates the scalability and transferability of such measures to the harvest block level. Models were trained using 38 plots across two sites dominated by Douglas-fir, then expanded to ten harvest blocks, and transferred to eight blocks from two sites without training data before being compared against multiple independent block-level estimates. Model results showed root mean square errors of 35% and 38% for merchantable and non-merchantable volumes, respectively. Merchantable volume estimates in blocks with training had average absolute differences from the harvest scale (9–34%) similar to transferred blocks without training (15–20%). Non-merchantable model results were also similar in both trained and transferred harvest blocks, with the pre-harvest model results having lower differences from the post-harvest geospatial versus field surveys. The results from this study show promise for hybrid methods to improve estimates of merchantable wood volume compared to conventional forest cover data approaches, and provide the ability to predict non-merchantable volumes within the range of accuracy of post-harvest residue survey methods.

**Keywords:** LiDAR; enhanced forest inventory; area-based approach; individual tree approach; merchantable wood volume; non-merchantable wood volume; logging residues



**Citation:** Kelley, J.; Trofymow, J.A.; Bone, C. Combining Area-Based and Individual Tree Metrics for Improving Merchantable and Non-Merchantable Wood Volume Estimates in Coastal Douglas-Fir Forests. *Remote Sens.* **2022**, *14*, 2204. <https://doi.org/10.3390/rs14092204>

Academic Editor: Carlos Alberto Silva

Received: 28 March 2022

Accepted: 30 April 2022

Published: 5 May 2022

**Publisher's Note:** MDPI stays neutral with regard to jurisdictional claims in published maps and institutional affiliations.



**Copyright:** © 2022 by the authors. Licensee MDPI, Basel, Switzerland. This article is an open access article distributed under the terms and conditions of the Creative Commons Attribution (CC BY) license (<https://creativecommons.org/licenses/by/4.0/>).

## 1. Introduction

Forests are a critical global resource, serving as the foundation for numerous national economies while at the same time driving the global carbon cycle [1,2]. Canadian forests are a critical component of this natural resource as they make up over 9% of the world's total forest cover [3]. As of 2018, a significant proportion (226 million hectares, or 65%) of these forests are considered actively managed, much of which has contributed over CAD 25 billion to the national GDP through industrial operations [3]. At the same time, forests play a critical role in the national and global carbon balance by potentially acting as landscape-level carbon sinks through conservation or targeted management activities [4] or acting as carbon sources due to anthropogenic disturbances such as harvesting [5] or natural disturbances such as wildfires [6].

An examination of the mitigation potential of managed forests in Canada showed that changes to management policies could increase the mitigation potential of forest lands by

45.1 Tg CO<sub>2</sub>e per year by 2050 [7]. In the province of British Columbia, similar changes in forest management practices (including producing longer-lived products, utilizing more harvested material, as well as utilizing harvest residues for bio-energy) were shown to have cumulative mitigation effects that could contribute up to 35% of the province's carbon reduction target by 2050 [8]. These relatively small changes in management practices have been recognized to increase the positive mitigation potential of managed forests [9,10]. Furthermore, the Intergovernmental Panel on Climate Change (IPCC) recognizes several management options to increase the climate change mitigation potential of forests [4], including reducing deforestation, increasing afforestation, conducting selected silvicultural practices, and increasing the utilization of cut forest material for use as products in the bioeconomy [11].

In response to political pressures to reduce carbon emissions, many forest companies in Canada have begun utilizing waste from the milling process as a source for on-site bio-energy production [12]. This process involves using solid wood waste from manufacturing (i.e., chips, shavings, or sawdust) or black liquor produced from pulp mills to generate electricity that can be used on-site or sold to electricity markets [13]. It has been estimated that national bioenergy production could displace emissions from energy usage by 27 Mt CO<sub>2</sub>e per year. However, this is most effective when bioenergy displaces energy produced from fossil fuels instead of other energy sources such as hydroelectricity [14]. While most of the bio-energy production in the context of forest processing has been utilizing feed sources (i.e., fuels) from milling waste, a relatively underutilized source of bio-material is residues from logging [13].

In general, logging residues from harvest sites (i.e., non-merchantable trees and log processing remnants that are cut but left in a harvest block) are piled and burned or left dispersed across a harvest block [15]. Logging residues are a viable feed source [16], although the amount of available supply remains generally unknown until after harvest is completed, creating challenges for increasing their utilization [12]. One solution to enhance the industry's ability to increase logging residue use is to refine the prediction and forecasting of non-merchantable timber volumes. Logging residue estimates could be improved from methods that provide coarse-scale regional estimates [12,17] towards approaches that focus on operational scales such as individual harvest blocks.

Remote sensing and spatial modelling have provided successful approaches for conducting logging residue measurements [18–20]. Satellite imagery, for example, has been used to conduct national-level assessments of potential biomass available from logging residues [12] and salvage after wildfires [21]. Additionally, geospatial models and spatially explicit carbon models have been used to estimate the availability of woody biomass for bioenergy [17,22]. However, several factors currently constrain the capacity for remote sensing and spatial analysis at the individual harvest block, including the use of moderate resolution ( $\geq 250$  m) remote sensing data, variable definitions of logging residues, and analysis at the spatial scale of forest management units.

More recent remote sensing solutions, such as enhanced forest inventory (EFI) methods, have been developed that overcome issues of resolution to allow for estimating forest attributes, including merchantable volume, at operational scales such as individual harvest blocks. Such methods utilize high-resolution remote sensing data, such as LiDAR or optical imagery, and can be generally characterized into one of two approaches that differ in scale: area-based (AB) and individual tree (IT).

The AB approach creates a generalized statistical model that accounts for the entire forest canopy profile within a rasterized grid cell. LiDAR data and a network of training ground plots are used to develop a statistical model using either parametric [23–25] or non-parametric [26–28] methods. Once a plot level model is developed, it can then be applied to the larger area of interest, provided that it has similar characteristics as the training plots, by using a rasterized grid of LiDAR metrics similar to those used in the model development [29]. A general advantage of the AB approach is that both the dominant canopy trees and the sub-canopy trees are typically accounted for, given that appropriate

LiDAR densities exist when developing the attribute models. While several studies have implemented the AB approach successfully with an improved level of accuracy over traditional inventories [26,30,31], some results indicate that the AB approach performs better in structurally homogenous even-aged stands, which can present challenges when modelling attributes such as wood volume in more complex stands [24,25].

Alternatively, the IT approach focuses on the larger trees that dominate images of the top of the forest canopy. IT approaches generally utilize image segmentation techniques to identify and delineate the crowns of individual trees. Some of these methods delineate tree crowns from a LiDAR canopy height model (CHM) up from the space between crowns [32], down from an initial treetop point [33], or directly from the point cloud itself [34]. The main advantage of using LiDAR data in the IT approach is that a more direct measurement of tree attributes, such as height and crown area, can be obtained. Furthermore, IT segmentation can classify tree species when combined with appropriate imagery [32]. As well, attributes such as species, height, and crown area can be used to model additional attributes, such as diameter at breast height [35], which ultimately could lead to individual tree volume measurements using allometric equations [36]. These estimates can then be summed up to the stand, harvest block, or landscape level for which there is data coverage and similar forest characteristics as the training data. The major limitation of the IT approach is a sensitivity to errors of omission and commission, as it is limited to segmenting crowns from the larger upper canopy trees only [37]. However, summary metrics produced from an IT approach could provide valuable additional stand information, such as tree density or spectral characteristics, to an AB modelling approach.

Several studies have proposed a hybrid EFI approach which combines methods from both the AB and IT approaches, and most have taken similar steps of summarizing metrics calculated for the ITs into a grid similar to the AB predictor metrics [23,37–39]. The main premise of this approach is that the inclusion of IT metrics allows for potential weighting towards the larger trees that make the largest contributions to total volumes. However, a limitation of using a hybrid method is the significantly increased processing time, as IT analysis needs to be completed and summarized into appropriate metrics before the model fitting can be continued, requiring considerable processing time for large areas. Yet, estimating the non-merchantable volume component presents a unique case where the increased times may be justified as IT variables, such as stocking density and crown area, could provide important information about the amount of non-merchantable material available.

While a hybrid approach has been shown to improve forest attribute estimates compared to independent AB and IT approaches, applications of EFI methods have generally focused on merchantable volume components, with little effort to estimate the non-merchantable components [24,26,33]. Additionally, limited research has been conducted to explore how EFI models scale to a harvest block and transfer to areas of similar conditions without prior training [26,27]. This is desirable as creating a transferable model to other harvest blocks would reduce the cost of establishing ground sample plots with every new harvest block. Traditionally, EFI models are fit using sample plot data and then expanded to a larger area or transferred to a new area and evaluated against additional sample plot data, which can be limited by sampling density and distribution of plots [27]. Alternatively, all merchantable wood transported off-site is scaled after harvest, allowing for a complete census of merchantable volume, which can then be compared to EFI model results on a harvest block-level [26].

Similarly, the traditional method to measure and estimate non-merchantable volumes in a harvest block uses sample estimates from plots or transects and then scaling up sample estimates to the stratum or block-level [40]. These methods are limited because they also depend on the number and location of sample plots, which underestimate total non-merchantable volumes [15]. However, recent methods have been developed to conduct a complete census of non-merchantable volume in the harvest block using a semi-automated log delineation method (SLD) [41].

Given the shortcomings described above, this study aims to understand the application of an enhanced forest inventory method that combines the area-based and individual tree approaches to develop hybrid models (hereafter referred to as the HB models) that estimate the amount of pre-harvest merchantable and non-merchantable material that would result from harvesting operations. To accomplish this, we will address the following question: to what extent are estimates obtained using an HB model scalable to the harvest block level and transferable to blocks without plot level training data? In answering this, we also seek to understand how HB models select for specific individual tree metrics by examining the overall importance of both area-based and individual tree-based predictor metrics.

## 2. Materials and Methods

### 2.1. Study Area Descriptions

The study area for this research is composed of five sites in Pacific coastal forests located on Vancouver Island, British Columbia (B.C.), Canada. All sites are located within various subzones of the Coastal Western Hemlock biogeoclimatic zone [42]. In total, 18 sample blocks across the five sites were examined in this study.

#### 2.1.1. Oyster River

The Oyster River (OR) site, located northwest of Courtenay, B.C. (Figure 1), was part of Fluxnet Canada's network of monitoring stations from 1997 to 2010, a network of eddy-covariance flux towers across Canada in various forest types used to continuously monitor carbon exchanges between the forest and atmosphere [43]. A central portion of this site was planted in 1949 as a second-growth Douglas-fir (*Pseudotsuga menziesii*) dominated stand with some western hemlock (*Tsuga heterophylla*), western redcedar (*Thuja plicata*), and red alder (*Alnus rubra*) (Table 1) [5]. The average estimated site index of these stands was 36 m, and the elevation at this site ranged from 259 to an average of 335 m, while the slope is moderate to high (Table 1). Between 2010 and 2011, this central portion of the site was harvested in four blocks—WH017, WH017a, WH017b, and WH017c [15].

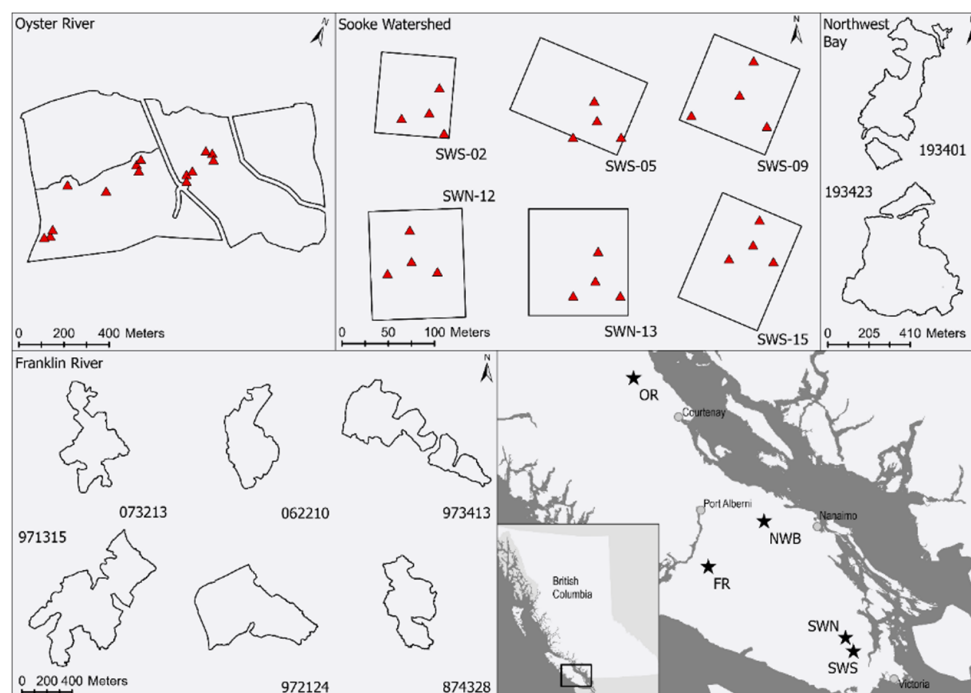


**Figure 1.** Study site map showing layouts of block boundaries (black lines) and sample plot locations (red triangles) at Oyster River (OR), Sooke Watershed South (SWS) and Sooke Watershed North (SWN), Northwest Bay (NWB), and Franklin River (FR). All sites are located in Douglas-fir dominated sites on Vancouver Island, with central site locations shown (stars) in the lower right panel.

**Table 1.** Sample block site descriptions including earliest estimated establishment date (Est. Date), major species composition, main stand estimated site index (m) (site height at 50 years age at DBH), average block elevation (m ASL), average block slope (degrees) for blocks located at the Oyster River (OR), Sooke Lake Watershed South (SWS), Sooke Lake Watershed North (SWN), Northwest Bay (NWB), and Franklin River (FR) sites. Major species include Douglas-fir (Fd), western hemlock (Hw), western red cedar (Cw), and amabilis fir (Ba). Est. Date determined through tree core analysis at OR, SWS, SWN and through existing forest inventories at NWB and FR.

Site	Block	Est. Date	Species	Site Index	Elevation	Slope	Harvest Year
OR	WH017	1949	FdHwCw	37.0	259	10	2011
OR	WH017a	1949	FdHwCw	36.0	328	11	2010
OR	WH017b	1949	FdHwCw	34.0	335	11	2011
OR	WH017c	1949	FdHwCw	37.0	275	7	2011
SWS	02	1960	FdHwCw	38.8	296	20	-
SWS	05	1892	FdCw	25.6	220	8	-
SWS	09	1816	FdCw	24.3	347	25	-
SWN	12	1949	FdCwHw	33.4	348	8	-
SWN	13	1898	FdCwHw	29.9	250	12	-
SWN	15	1695	Fd	29.9	491	21	-
NWB	193401	1962	FdCwHw	28.0	456	10	2014
NWB	193423	1959	FdHwCw	28.0	612	15	2014
FR	073213	1943	HwFd	34.2	281	15	2019
FR	062210	1945	FdHwCw	31.2	132	17	2018
FR	973413	1948	FdHw	29.5	316	23	2018
FR	971315	1941	HwFdBa	29.4	348	19	2019
FR	972124	1945	HwFd	27.5	192	17	2019
FR	874328	1943	FdHw	29.5	167	24	2019

### 2.1.2. Sooke Lake Watershed

The Sooke Lake watershed area is located near Victoria, B.C. and hosts two sites: Sooke Lake Watershed South (SWS) and Sooke Lake Watershed North (SWN) (Figure 1). Located at each site are young (est. 1960/1949), mature (est. 1892/1898), and old-growth (est. 1816/1695) stands (Table 1) being monitored as part of the Coastal Forest Chronosequence project [44,45]. Douglas-fir dominates the stands with additional western redcedar and western hemlock components and estimated site indices ranging from 24 to 39 m (Table 1). The average elevation at these sites ranged from 220 to 347 m at SWS and 250 to 491 m at SWN, and both sites had a range of slopes from moderate to very steep (Table 1). There was no harvesting in the three blocks at SWS or SWN. However, a nested sample design in which smaller inventory plots were nested inside larger stem-mapped demographic blocks [46] allowed for a simulated harvest to be conducted, as described below, and post-harvest block-level data to be calculated.

### 2.1.3. Northwest Bay

The Northwest Bay (NWB) site is located west of Nanaimo, B.C. (Figure 1), and had two blocks that were harvested in 2014 [40]. Prior to harvest, both blocks were primarily second-growth Douglas-fir with lesser amounts of western hemlock and western redcedar (Table 1). At NWB 193401, the stands were established between 1962 and 1965 and had site indices ranging from 18 to 28 m with strong slopes (Table 1). NWB 193401 was higher in elevation (456 m) than most blocks at the OR, SWS, and SWN sites, although lower than SWN 15 (Table 1). At NWB 193423, the stands were established between 1959 and 1980 with site indices ranging from 21 to 28 m and a slightly steeper slope than NWB 193401 (Table 1). The average elevation at NWB 193423 (612 m) was the highest of any blocks and was more than 150 m higher than NWB 193401 (Table 1). Both NWB 193401 and 193423 were harvested over the summer and fall of 2014 [41].



#### 2.1.4. Franklin River

The Franklin River (FR) site is located south of Port Alberni, B.C. (Figure 1). The FR blocks were composed of second-growth forests established between 1941 and 1948, and the main species present were mixtures of Douglas-fir, western hemlock, and western redcedar. However, some blocks had western hemlock as the dominant species and Douglas-fir as the secondary species, and one block included additional components of amabilis fir (*Abies amabilis*) (Table 1). The FR blocks had some of the lowest elevations of all sample blocks, but the overall range (132–348 m) was comparable with the other sites (Table 1). Alternatively, the slopes in the FR blocks were some of the highest (15–24°) but still within the range of other sites (Table 1). Harvesting of the six blocks at the FR site occurred between 2018 and 2019.

#### 2.2. Spatial Data

Spatial data for this study included pre-harvest LiDAR and imagery data, post-harvest imagery and photogrammetric point clouds, as well as pre- and post-harvest spatial boundaries. All spatial data were projected into a common coordinate system of NAD 1983 UTM zone 10n (EPSG: 29610), and block boundaries used to clip data to areas of interest were buffered by 100 m to limit the impacts of edge effects. Pre-harvest LiDAR acquisitions were performed in 2008 at the OR site (Leica ALS50-II, avg 3.74 points m<sup>-2</sup>) [47], 2012 at the SWS and SWN sites (Terra Remote Mark III, up to 70 points m<sup>-2</sup>) [48], 2011 at the NWB site (Terra Remote Mark III, avg 15 pts m<sup>-2</sup>) [15], and in 2016 at the FR site (Riegl LMS-Q780, avg 12 pulses m<sup>-2</sup>) (S. Platt—Western Forest Products, personal communication, 10 January 2020) (Table 2). LiDAR points from each site were classified into ground and non-ground points by vendors using various versions of the Terrascan software (Terrasolid, v021.023). All LiDAR point clouds were checked for errors such as duplicated points or air hits above the canopy using the lidR package in R [49]. Point density was calculated using a 20 m resolution raster and summarized each block as the average of cells with centroids within the block boundaries (Table 2). Point clouds were then normalized into heights above ground to remove the effects of local topography using the lidR package and a triangular irregular network [49].

**Table 2.** Point cloud and imagery characteristics and acquisition years. \* Note imagery from SWN-15 from 2013 similar to SWS.

Site	Point Density	Image Resolution (m)	LiDAR (Image) Year
Pre-harvest			
OR	6.9	1.0	2008 (2007)
SWS	3.7	0.2	2012 (2013)
SWN	10.1	0.2	2012 (2012 *)
NWB	23.1	0.1	2011 (2011)
FR	52.2	0.1	2016 (2016)
Post-harvest			
OR	15.1	0.02	2011 (2012)
NWB	n/a	0.02	n/a (2016)
FR	n/a	0.02	n/a (2019)

Pre-harvest orthoimagery was also acquired for the OR (2007), SWS (2013), SWN (2012/2013), NWB (2011), and FR (2016) sites. All imagery contained three channels (red, green, and blue) and had various delivered spatial resolutions (Table 2). The imagery at the OR site had a timing offset from the LiDAR data, similar to imagery from the SWS site and SWN block 15 (Table 2). The imagery from SWN blocks 12 and 13 was collected coincidentally with the LiDAR, similar to image acquisitions for the NWB and FR sites (Table 2). Imagery collected separately from the LiDAR acquisitions showed differences in absolute positioning of identifiable features compared to the LiDAR data. To geo-rectify imagery data to the LiDAR positioning, individual treetop positions were determined

using image-based [32] and point cloud-based [49] methods. The treetop positions of large identifiable trees near the edge of gaps were used to rectify the imagery to match the absolute positioning of the LiDAR data with co-registration root mean square errors  $\leq 2$  m.

Post-harvest very high resolution (2 cm) imagery was also acquired using remotely piloted aircraft for the independent geospatial survey of post-harvest residues in the OR (2011), NWB (2015), and FR (2019) sites. Images were used to generate orthomosaics and image point clouds for each site. All imagery contained three channels (red, green, and blue) and had various delivered spatial resolutions and positioning accuracies (Table 2). The imagery at the OR site [15] and NWB site [41] had been used in previous studies developing post-harvest geospatial survey methods, whereas imagery from the FR site was newly acquired for this study (Table 2).

### 2.3. Spatial Data Processing

#### 2.3.1. Pre-Harvest

A point thinning method was used to address the large range in average LiDAR point density between the different sites. This method randomly removed points from within a 25 m<sup>2</sup> window to a maximum density of 3 points m<sup>-2</sup> and produced consistent results across the entire block, particularly in areas of scan line overlap with the target density chosen based on the 25th percentile of the calculated point densities in each block. Thinning was performed to produce a similar point cloud structure through all study sites when generating point cloud metrics, as Tompalski et al. [27] found that non-parametric implementations of the AB approach are sensitive to differences in point cloud structure among different sites. Canopy height models (CHMs) were produced using the thinned point clouds and a pit-free algorithm [50], with intermediate TIN surfaces produced at 2, 5, 10, 15, 20, and 30 m, removing edges longer than 1.5 m.

Next, a series of IT metrics were calculated from the segmented trees, including the crown area, the 95th percentile of the IT LiDAR height, and the average pixel values from the three imagery channels. Before the average imagery values were calculated, each image was resampled to 0.5 m to match the spatial resolution of the CHMs. Next, a bright pixel mask was created using the green channel and selecting pixels with a green value higher than the ITs average green value [32]. The red, green, and blue channel averages were then calculated for pixels within each IT's bright pixel mask. Finally, IT metrics were summarized using a rasterized grid with a 20 m resolution, matching the area of sample plots (0.04 ha), such that the average was calculated for the height, area, and imagery metrics for all trees that had their tops within a particular raster cell. An IT density metric was also calculated for each cell as the number of IT tops divided by the cell area (0.04 ha).

A series of LiDAR metrics more common with traditional AB approaches was also generated using the same 20 m rasterized grid, similar in size to sample plots (0.04 ha). These predictor metrics included a combination of height, density, canopy cover, and statistical metrics similar to those produced and used by Kelley et al. [28]. In total, 34 AB metrics were created using the lidR package in R [49] to be included with the six IT metrics (Table 3). Additionally, all point clouds and IT segmentations were clipped to the same extent as the sample plots, and the same combination of 40 AB and IT metrics was generated at the plot level for the development of the HB model.

**Table 3.** Area based (AB) and individual tree (IT) style predictor metrics used for variable selection.

Class	Code	Description
AB	CanRelRatio	$((\text{mean ht} - \text{min ht}) / (\text{max ht} - \text{min ht}))$
AB	p1st_abv_2	Percentage 1st returns above 2 m
AB	p1st_abv_Mean	Percentage 1st returns above mean ht
AB	p1st_abv_Mode	Percentage 1st returns above mode ht
AB	Zaad	Average absolute deviation (AD) of ht
AB	Zl1	First L moment
AB	Zl2	Second L moment
AB	Zlcv	L-moment coefficient of variation
AB	Zlkur	L-moment kurtosis
AB	Zlskew	L-moment skewness
AB	Zmadmed	Median of the AD from the overall median
AB	Zmadmod	Median of the AD from the overall mode
AB	ZquadMean	Quadratic mean of ht
AB	zq10-95	Xth percentile of height distribution (10, 20, 25, 30, 40, 50, 60, 70, 75, 80, 90, 95)
AB	Zpcum1-9	Cumulative percentage of returns in the Xth decile (1–9)
IT	IT_TTDens	Individual tree density ( $\# \text{ ha}^{-1}$ )
IT	IT_z95	95th percentile of individual tree LiDAR points
IT	IT_crownarea	Individual tree crown area
IT	IT_redspec	Individual tree mean red channel
IT	IT_greenspec	Individual tree mean green channel
IT	IT_bluespec	Individual tree mean blue channel

### 2.3.2. Post-Harvest

Processing of post-harvest imagery to detect dispersed and roadside residues for the OR and NWB blocks is described in detail in Trofymow et al. [15] and Trofymow et al. [40], respectively. At the FR site, post-harvest orthoimagery in each block was resampled to a 5 cm spatial resolution for use in the SLD algorithms. An averaged blue channel image was created using a two-pass mean filter with a window size of  $7 \times 7$  and  $31 \times 31$ , which was subtracted from the blue channel to create a normalized blue channel image [40] and used by the SLD algorithms to detect roadside and dispersed residues. At all sites, orthoimagery was used to manually delineate the boundary of residue piles and heavy accumulations. At the OR site, the differencing of a LiDAR-derived digital terrain model (DTM) and digital surface model (DSM) was used to calculate bulk pile volumes [15]. At both the NWB and FR sites, photogrammetric point clouds were edited to remove points from within the piles, and pseudo DTMs were created and differenced from DSMs created with the full point cloud to determine pile bulk volumes [41].

### 2.4. Training Data from Plots at the OR, SWS and SWN Sites

Data from sample ground plots at OR, SWS, and SWN were used as the training data for the HB model. During the 2009 growing season at the OR site, 14 circular sample plots with an area of 0.04 ha were measured following Canada's National Forest Inventory sampling guidelines [51]. Measurements recorded included species, diameter at breast height (DBH), and height for all trees  $\geq 1.3$  m in height within the plot areas. At the SWS and SWN sites, similar measurements were recorded for trees within sample plots (4 per block) during the 2014 growing season. Sample plots in SWS 09 were 0.04 ha in size, whereas plots in all other blocks at SWS and SWN were 0.03 ha.

Total and merchantable volumes in the plots were determined from individual tree volumes calculated using the tree species, DBH, and height data, as input to regional taper equations developed by Kozak [36]. For each tree, jurisdictional timber criteria and available timber cruise data helped determine the merchantability parameters, set as a 30 cm stump height, 10 cm top height, 12.5 cm minimum DBH, and a 10 m log length (Timber Pricing Branch, 2011). At the old-growth plots in SWS-09 and SWN-15, the minimum DBH limit was increased to 17.5 cm to match merchantability limits of coastal



old-growth stands [52]. The volume of each tree that met the merchantability limits was used to populate the initial merchantable volume pool (Figure 2). Next, sampled trees identified as dead standing had merchantable volumes transferred to the non-merchantable pool (Figure 2). A final merchantable volume net-down of 6% for conifer species and 9% for deciduous species was subtracted from each live tree's merchantable volume and added to the non-merchantable volume pool. The net-down values were determined from averaging species-specific reductions applied in available timber cruise data from the FR blocks.

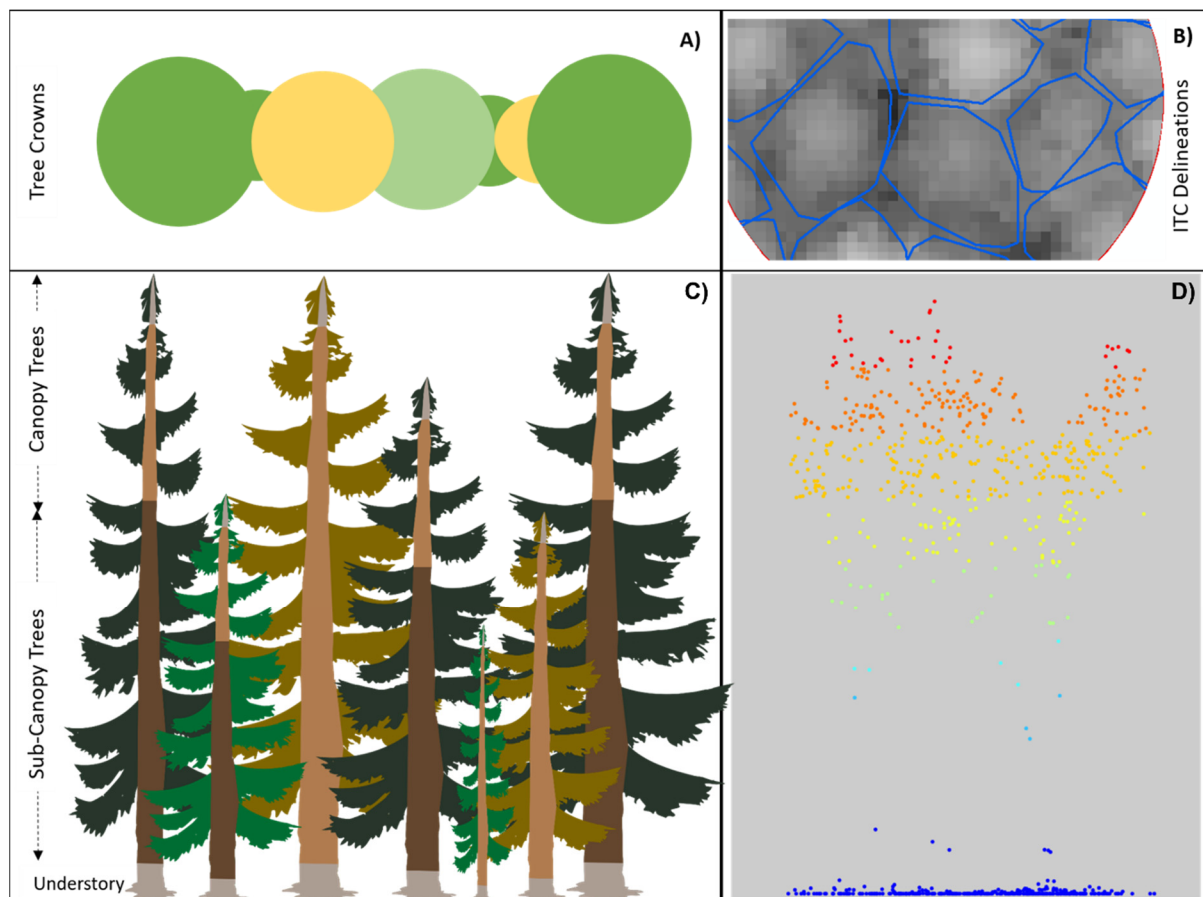


**Figure 2.** (A) Diagram depicting the areal appearance of the canopy and sub-canopy tree crowns; (B) data representations of an individual tree delineation for OR plot 11.3; (C) structure of a complex forest with live (dark and light green crown, respectively) and dead (yellow crown) trees that make up the canopy and sub-canopy. Also shown are the stem wood components of merchantable stem wood ( $\geq 12.5/17.5$  cm DBH and 10 m length) (dark brown), non-merchantable stem wood ( $\geq 10$  cm diameter and  $< 10$  m length) (light brown), and stumps and tops (grey). (D) Corresponding LiDAR point cloud for OR plot 11.3.

Tree volume that belonged to undersized stems ( $< 12.5/17.5$  cm DBH) (not including stumps or tops) and the short ( $< 10$  m) logs were used to populate the initial non-merchantable volume pool (Figure 2), followed by the addition of dead trees and the net-down portion of the live tree merchantable volume described above. Then, for each sample plot, the total merchantable and non-merchantable volumes for all trees were summed and plot merchantable and non-merchantable volume densities ( $\text{m}^3\text{ha}^{-1}$ ) calculated and used for the HB model training.

### 2.5. Hybrid Model Development

The forty combined metrics for each of the 38 sample plots were used in a Boruta feature selection routine to select a subset of training metrics for merchantable and non-

merchantable volume models. Boruta feature selection is a method popularly used for models with many predictor metrics and, more recently, in implementations of LiDAR EFI models [28,37]. First, the Boruta method adds copies of the predictor metrics that are randomly permuted noise metrics [53]. Next, over 1000 random forest (RF) iterations, the algorithm tracks the RF variable importance scores and calculates the z-scores for each expanded set of predictor metrics, comparing z-scores between the original metrics and the noise metrics [53]. The final selected metrics are those metrics that have a significantly higher z-score than the highest scoring noise variable.

RF models for both the merchantable and non-merchantable volume components were fit using the Boruta reduced predictor metrics. Models were trained using 1000 regression trees and the caret [54] and random forest [55] packages in R in a five-times repeated 10-fold cross-validation method [56]. This training method results in 50 independent cross-validation observations used to assess model performance by calculating the absolute, and relative root mean square error (RMSE) and bias [56]. Each model was then expanded to the block areas using the suite of raster-based predictor metrics. For each cell with a centroid within the block boundaries, the predicted volume density was multiplied by the cell area (0.04 ha), and the total block merchantable or non-merchantable volume was summed and divided by the total block area to calculate block-level densities ( $\text{m}^3\text{ha}^{-1}$ ) of predicted merchantable and non-merchantable volume.

#### 2.6. Sources of Block-Level Data for Testing Hybrid Models

The HB models were trained and parameterized using plot data from the OR, SWN, and SWS sites. The trained models were then expanded to the harvest blocks at the OR, SWN, and SWS sites and transferred to the harvest blocks at the NWB and FR sites, which had no prior training and were then tested against block-level independent data for all five sites. While the OR, NWB, and FR sites had post-harvest block-level measurements of merchantable and non-merchantable volumes, the demographic blocks at SWS and SWN were not harvested, thus a simulated harvest was conducted. The SWS and SWN demographic blocks recorded species and diameter measurements for all trees and heights for a subset of trees. For those trees missing height measurements, a Chapman–Richards function was used to estimate height with parameters fit using data from trees that had both height and diameter measurements similar to Kelley et al. [28] and Metsaranta et al. [57]. A simulated harvest was then performed for all trees in a block, and total merchantable and non-merchantable volumes were calculated using the same merchantability limits as described above for the sample plots.

Estimates of block-level merchantable volumes ( $\text{m}^3\text{ha}^{-1}$ ) derived from the HB models were compared to two independent sources of merchantable volume. The first came from traditional forest cover data used to calculate pre-harvest volumes in each block. The traditional forest cover data used was a mixture of polygonal inventories that were derived through air photo interpretation (for the SWS and SWN sites), such as the BC Vegetation Resource Inventory [58], or from internal industry inventories derived from timber cruising (for the OR, NWB, and FR sites). The second source of merchantable volume data at the OR, NWB, and FR sites, provided by the operating companies, was the scaled volume for logs transported to a log sort. Therefore, the calculated merchantable volumes from the simulated harvest of the demographic blocks at the SWS and SWN sites were used as a proxy for the harvest scale volumes.

Estimates of modelled block-level non-merchantable volumes ( $\text{m}^3\text{ha}^{-1}$ ) at the OR, NWB, and FR sites were compared to two independent sources of post-harvest residue volumes. The first source was the provincial standard waste and residue survey (WRS) sample plots measured on each block post-harvest [59]. The second used a geospatial semi-automated log delineation (SLD) method for dispersed residues while bulk pile volumes and packing ratios were used to determine accumulations and piled residues (P method) [40,41] to perform a complete census of residues in the entire post-harvest block. The harvest block and WRS sampling stratum boundaries were digitized for all blocks

using very high-resolution orthoimages. Non-merchantable WRS volume estimates were determined using the digitized stratum areas and the average stratum densities from WRS sampling plots. Total block density ( $\text{m}^3\text{ha}^{-1}$ ) was calculated by summing all stratum totals and dividing by the total block area [15]. Non-merchantable volume estimates were also determined using the SLD method for the dispersed and light-roadside stratum and the P method for the heavy-roadside and piled stratum [40,41]. The total block densities were determined by summing SLD and P stratum totals (SLDP method) and dividing by the total block area [41]. At the SWS and SWN sites, the calculated non-merchantable volume from the simulated harvest of the demographic blocks was used as a proxy for the SLDP volume measurements.

### 2.7. Hybrid Model Testing and Comparisons

For each block, the total summed merchantable volume from the pre-harvest HB model, pre-harvest forest cover, and post-harvest scale was divided by the area of the digitized block boundaries to determine total merchantable volume densities ( $\text{m}^3\text{ha}^{-1}$ ). The block volume densities for the two pre-harvest sources were compared to the post-harvest scale in paired *t*-tests [37]. The Shapiro–Wilk normality test was used to investigate if the differences between sources were normally distributed. Additionally, the difference between the post-harvest scale and each of the two pre-harvest methods (post-harvest–pre-harvest) was calculated for comparison.

Total non-merchantable volumes were also summed to a block total divided by the digitized area ( $\text{m}^3\text{ha}^{-1}$ ) for the pre-harvest HB model results, the post-harvest WRS estimates, and the post-harvest SLDP estimates. Similar to the merchantable volumes, paired *t*-tests were used to compare the pre-harvest HB model with the two post-harvest methods, and the Shapiro–Wilk test [60] was used to test for normality of the method differences. Finally, the differences between each of the two post-harvest methods and the pre-harvest model results (post-harvest–pre-harvest) were calculated for comparison.

## 3. Results

### 3.1. Variable Selection

The Boruta feature selection method reduced the original 40 metrics to 16 metrics for the merchantable volume component (Figure 3). The average variable importance scores ranged from 2.5 to 7.7 for the selected variables, which were dominated mainly by height metrics. The average 95th percentile of individual tree (IT) height was the only IT metric selected for the merchantable volume component. However, it scored higher on average than similar maximum height metrics (zq90 and zq95) from the traditional AB metrics and was within the top ten selected metrics (Figure 3). For the non-merchantable component, the Boruta method resulted in a more considerable reduction down to 10 metrics from the original 40 (Figure 3). The average importance scores for the selected metrics ranged from 2.9 to 4.3 and contained a mixture of all types of predictor metric classes (height, density, statistical, and IT). The highest scoring IT variable was the average blue channel from the tree crowns and was the third-highest scoring variable overall for the non-merchantable volume component (Figure 3).

### 3.2. Model Fitting and Expansion

The hybrid (HB) merchantable volume model showed an  $R^2$  value of 0.75 with a cross-validated (CV) root mean square error (RMSE) of  $240.11 \text{ m}^3\text{ha}^{-1}$  (34.7%) and a bias of  $-45.07 \text{ m}^3\text{ha}^{-1}$  (−6.5%). Examining the plot level model predictions against the measured observations shows a variable bias, with predictions being the furthest from observations in the plots with the largest observed volumes, SWS 09 and SWN 15 (15-S) (Figure 4). The non-merchantable volume HB model showed a lower  $R^2$  value of 0.49, but the CV RMSE of  $52.28 \text{ m}^3\text{ha}^{-1}$  (38.0%) was in a similar relative range as the merchantable volume model. The CV bias of  $-2.14 \text{ m}^3\text{ha}^{-1}$  (−1.6%) for the non-merchantable volume was smaller than the merchantable model. The plot-level model predictions versus the observed

measurements show a higher variable bias than the merchantable volume model, although the largest discrepancies were also in the plots with the highest observed non-merchantable volumes (Figure 4).

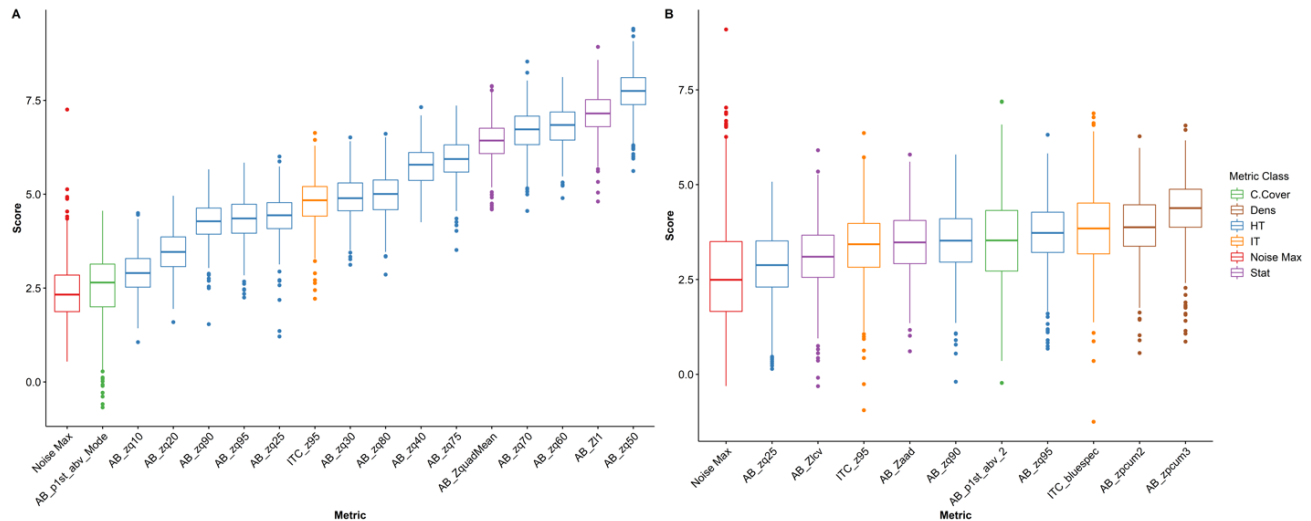


**Figure 3.** Boruta variable selection results showing the distribution of variable importance scores of selected metrics for the merchantable volume component (A) and non-merchantable volume component (B). Color indicates metric classes of canopy cover (C. Cover) (green), density (Dens) (brown), height (HT) (blue), individual tree (IT) (orange), statistical (Stat) (purple), and the highest-scoring noise variable (Noise Max) (red).

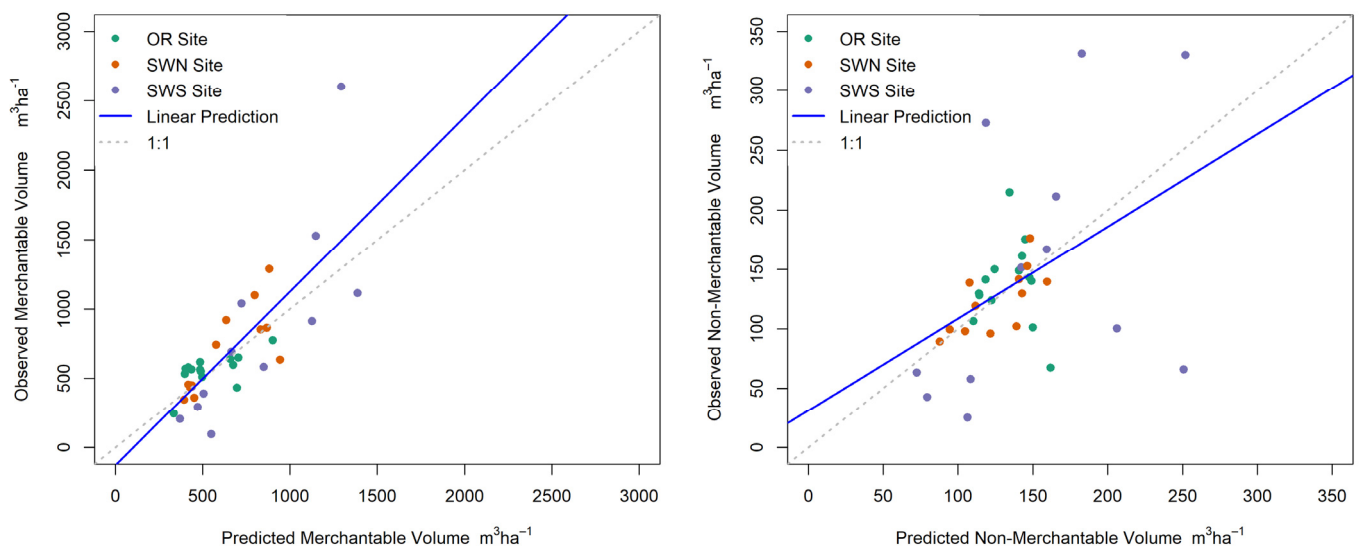


**Figure 4.** Observed plot level vs. RF predicted merchantable (left) and non-merchantable (right) volumes at the Oyster River (OR) (green), Sooke Lake Watershed South (SWS) (purple), and Sooke Lake Watershed North (SWN) (orange) sites.

Applying the merchantable volume HB model to the block level showed that the average merchantable volume in the OR blocks,  $538 \text{ m}^3\text{ha}^{-1}$ , was slightly lower than averages at the other sites with plot-level training data (SWS =  $795 \text{ m}^3\text{ha}^{-1}$ , SWN =  $608 \text{ m}^3\text{ha}^{-1}$ ). However, this is due mainly to the old-growth blocks, SWS-09 and SWN-15 (Table 4). The NWB site had the lowest average merchantable volume model estimate of  $339 \text{ m}^3\text{ha}^{-1}$ , and the average at the FR site of  $655 \text{ m}^3\text{ha}^{-1}$  was within the range of the other blocks that had training data. Similarly, the non-merchantable volume model showed a lower average

value in the OR site ( $124 \text{ m}^3\text{ha}^{-1}$ ) than in the other training sites ( $\text{SWS} = 144 \text{ m}^3\text{ha}^{-1}$ , and  $\text{SWN} = 129 \text{ m}^3\text{ha}^{-1}$ ). However, while the NWB site still showed the lowest average non-merchantable volumes ( $120 \text{ m}^3\text{ha}^{-1}$ ), the difference from the range of the training sites was not as large. Additionally, the non-merchantable volumes estimated in the FR sites had shown on average  $145 \text{ m}^3\text{ha}^{-1}$ , which was slightly higher than the highest value in the training sites.

**Table 4.** Block digitized areas (ha) and block-level HB random forest model estimates of merchantable ( $\text{m}^3\text{ha}^{-1}$ ) and non-merchantable volumes ( $\text{m}^3\text{ha}^{-1}$ ).

Site	Block	GIS Area	Merchantable Volume	Non-Merchantable Volume
OR	WH017	11.44	607.63	131.02
OR	WH017a	24.29	518.36	126.95
OR	WH017b	18.16	538.49	130.23
OR	WH017c	22.59	579.99	128.43
SWS	02	0.704	352.54	78.35
SWS	05	1.066	877.71	176.05
SWS	09	1.000	1156.14	178.38
SWN	12	1.188	406.05	130.02
SWN	13	1.240	670.08	140.23
SWN	15	1.139	749.32	116.19
NWB	193401	11.59	352.21	123.97
NWB	193423	20.30	363.03	128.66
FR	073213	17.58	774.20	155.55
FR	062210	16.64	606.05	138.79
FR	973413	27.95	615.02	136.68
FR	971315	36.58	550.36	142.80
FR	972124	29.92	635.92	147.93
FR	874328	16.35	750.96	150.26

### 3.3. Comparison of HB Model Estimates with Block-Level Data

#### 3.3.1. Merchantable Volumes

Pre-harvest merchantable volume estimates from forest cover data were consistently lower on average in all blocks than the actual or simulated harvest scale data, with the largest average absolute difference being at the SWS, SWN, and NWB sites (Table 5) (Figure 5a). Paired *t*-test results showed a significant difference between the forest cover and harvest scale data ( $t = -2.65$ ,  $p$ -value = 0.017). In addition, the pre-harvest HB model estimates showed more variability of over and under-estimations of the harvest scale compared to the forest cover data. On average, the HB model overestimated merchantable volumes at the SWS and SWN sites and showed underestimates at all other sites (Table 5). In contrast to the forest cover data, the results from paired *t*-test comparison of merchantable volume from the harvest scales to the HB model indicated no significant difference between the means of the two methods ( $t = 1.30$ ,  $p$ -value = 0.211). On average, across the OR, NWB, and FR blocks, the absolute difference in merchantable volume between the harvest scale and the forest cover was 21% of the average harvest scale, whereas, for the HB model estimates, the average absolute difference was 14% of the average harvest scale (Figure 5a).



**Table 5.** Block merchantable volumes ( $\text{m}^3\text{ha}^{-1}$ ) for the post-harvest scale (HS), pre-harvest forest cover (FC), pre-harvest hybrid model (HB), and differences in pre-harvest estimates from post-harvest validation. Average differences use the absolute value of block differences. SE—standard error. \* Note: HS values for SWS and SWN were simulated using field measurements for all trees in the block. All blocks  $n = 12$  excludes HS values for SWS and SWN.

Site	Block	HS Volume	FC Volume	HB Volume	FC-HS Volume	HB-HS Volume
OR	WH017	647	559	608	−88	−40
OR	WH017a	564	559	518	−5	−46
OR	WH017b	656	337	538	−319	−118
OR	WH017c	557	559	580	2	23
OR	Avg (SE)	606 (26)	504 (56)	561 (20)	104 (75)	56 (21)
SWS	02	270 *	533	353	263	83
SWS	05	946 *	672	878	−274	−69
SWS	09	994 *	741	1156	−253	162
SWS	Avg (SE)	737 (234)	649 (61)	795 (236)	264 (6)	104 (29)
SWN	12	293 *	396	406	103	113
SWN	13	436 *	598	670	162	234
SWN	15	976 *	497	749	−479	−226
SWN	Avg (SE)	568 (208)	497 (58)	608 (104)	248 (117)	191 (39)
NWB	193401	419	241	352	−178	−67
NWB	193423	519	202	363	−317	−156
NWB	Avg (SE)	469 (50)	222 (20)	358 (5)	248 (70)	112 (45)
FR	073213	825	550	774	−275	−51
FR	062210	672	582	606	−90	−66
FR	973413	738	569	615	−169	−123
FR	971315	755	700	550	−55	−205
FR	972124	838	841	636	3	−202
FR	874328	708	560	751	−148	43
FR	Avg (SE)	756 (27)	634 (47)	655 (36)	123 (39)	115 (30)
Blocks $n = 18$	Avg (SE)	656 * (51)	539 (38)	617 (48)	177 (31)	112 (16)
Blocks $n = 12$	Avg (SE)	658 (36)	522 (52)	574 (37)	137 (34)	95 (19)

### 3.3.2. Non-Merchantable Volumes

Pre-harvest estimates of non-merchantable volume from the HB model were continuously higher on average than the post-harvest estimates from the waste and residue survey (WRS) (Table 6) (Figure 5b). The paired  $t$ -test across all blocks showed that the means between these two methods were significantly different ( $t = 7.12$ ,  $p$ -value  $< 0.001$ ). Alternatively, compared to the semi-automated log delineation plus piles (SLDP) estimates, the HB model results are more variable, with the majority of blocks showing model results to be lower than SLDP estimates (Table 6). The paired  $t$ -test across those blocks with an SLDP method applied showed no significant difference between method means ( $t = -0.34$ ,  $p$ -value = 0.736). Across the OR, NWB, and FR blocks, the average absolute difference between the WRS and HB model results was 63% of the WRS average, where the average absolute difference between the SLDP and HB model results across all blocks was much lower and only 20% of the SLDP average (Table 6) (Figure 5b).

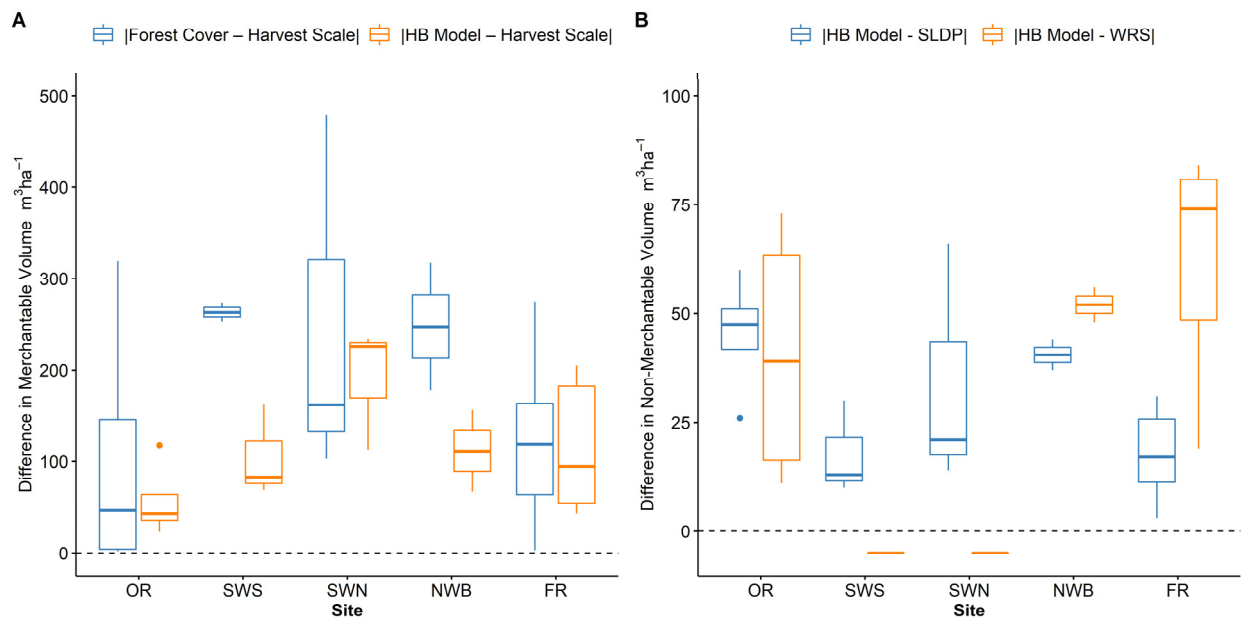


**Figure 5.** (A) Block merchantable volume ( $\text{m}^3\text{ha}^{-1}$ ) absolute difference of post-harvest scale (HS) from pre-harvest forest cover (FC) (blue) and pre-harvest hybrid model (HB) (orange). (B) Block non-merchantable volume ( $\text{m}^3\text{ha}^{-1}$ ) absolute difference from pre-harvest hybrid model (HB) for the post-harvest semi-automated log delineation plus piles (SLDP) (blue) and the post-harvest waste and residue survey (WRS) (orange). Note: HS and SLDP values for SWS and SWN were simulated using field measurements for all trees in the block. WRS values for SWS and SWN are N/A (-1).

**Table 6.** Block non-merchantable volumes ( $\text{m}^3\text{ha}^{-1}$ ) for the post-harvest waste and residue survey (WRS) estimate, post-harvest semi-automated log delineation plus piles (SLDP) residue estimate, pre-harvest hybrid (HB) model predictions, and differences between pre-harvest estimates and post-harvest values. Average volume differences use the average absolute difference. SE—standard error. \* Note: SLDP values for SWS and SWN were simulated using field measurements for all trees in the block. All blocks  $n = 12$  excludes values for SWS and SWN.

Site	Block	WRS	SLDP	HB Model	HB-WRS	HB-SLDP
OR	WH017	120	157	131	−11	26
OR	WH017a	67	174	127	−60	47
OR	WH017b	58	178	130	−73	48
OR	WH017c	110	189	128	−18	60
OR	Avg (SE)	89 (15)	175 (7)	129 (1)	40 (15)	46 (7)
SWS	02		49 *	78		−30
SWS	05		163 *	176		−13
SWS	09		168 *	178		−10
SWS	Avg (SE)		127 (39)	144 (33)		18 (6)
SWN	12		109 *	130		−21
SWN	13		74 *	140		−66
SWN	15		130 *	116		14
SWN	Avg (SE)		104 (16)	129 (7)		34 (16)

Table 6. Cont.

Site	Block	WRS	SLDP	HB Model	HB-WRS	HB-SLDP
NWB	193401	76	87	124	−48	−37
NWB	193423	72	85	129	−56	−44
NWB	Avg (SE)	74 (2)	86 (1)	126 (2)	52 (4)	40 (3)
FR	073213	75	166	156	−81	10
FR	062210	58	158	139	−80	19
FR	973413	117	167	137	−19	31
FR	971315	59	146	143	−84	3
FR	972124	80	133	148	−68	−15
FR	874328	108	178	150	−42	28
FR	Avg (SE)	83 (10)	158 (7)	145 (3)	62 (11)	18 (4)
Blocks <i>n</i> = 18	Avg (SE)		140 * (10)	137 (5)		29 (4)
Blocks <i>n</i> = 12	Avg (SE)	84 (7)	152 (10)	137 (3)	53 (7)	31 (5)

#### 4. Discussion

This study demonstrates the utility of a hybrid (HB) enhanced forest inventory modelling approach for estimating merchantable and non-merchantable timber volumes at the harvest block level. Individual tree (IT) metrics were ranked higher than Boruta noise variables in both HB models, and were among the top three ranked metrics for the non-merchantable model (Figure 3b). For the merchantable volume HB model, selected metrics were mostly composed of height percentiles, including the selected IT metric (Figure 3a).

The selected metrics were similar to other applications of traditional area-based (AB) models [25,26,61] and HB models [39] that estimate merchantable or total forest volume, where height percentile metrics were consistently the highest-ranked or final selected metrics. One of the highest-ranked metrics for the non-merchantable HB model was the IT blue channel metric (Figure 3b). The high ranking of this metric is believed to be driven by ITs that are dead standing and made up entirely of non-merchantable wood, as was seen in sample plots at SWS 05. Interestingly, using the blue image channel from RGB imagery is similar to the procedures in the semi-automated log delineation (SLD) method to detect post-harvest logging residues [41].

Despite relying on a limited number of training sample plots (38), HB model fits for both merchantable and non-merchantable volume components with RMSE values of 34.7% and 38.0%, respectively, were similar to total or merchantable volume estimates from other studies in complex coniferous forests using non-parametric modelling (RMSE: 23.3–31.4% [61]; RMSE: 17.9% [62]; RMSE: 33.2% [56]). For example, White et al. [26] utilized 788 sample plots to fit an AB model estimating merchantable volumes in Alberta with an RMSE of 26%, which was applied to 272 harvested stands, and Kankare et al. [39] utilized 254 sample plots to fit an HB style model in coniferous forests of southern Finland with RMSEs ranging from 26.4–34.0%. In addition, the recent implementation of a combination approach in pine forests utilized 1680 training plots to create HB style models of volume that had normalized RMSE values ranging from 34.6 to 42.6% and were applied to over 10,290 km<sup>2</sup> of forested area in the southern United States [37].

The results from this study also highlight the potential for the transferability of EFI models. The HB merchantable volume model results had average absolute differences of 9–34% of the harvest scale in harvest blocks with available plot-level training data (Table 5). When the HB model was transferred to those harvest blocks without pre-harvest plot-level training data, the average absolute difference from the harvest scale was within a similar range of 15–24%. A sample plot analysis of model transferability found that, using the same LiDAR acquisition, models trained in one area could be successfully transferred to similar

forest areas with no major increases to plot-level RMSE [27]. However, Kotivuori et al. [63] found that both forest structure and LiDAR sensor had considerable effects on volume model accuracy. For this study, data acquisitions took place over several years with numerous sensor platforms and differing positional accuracies. The fusion of these data has potentially increased uncertainty of model estimates through compounding errors, however as an initial application the HB model results are still promising. A formal analysis of the impacts of data fusion on hybrid models would be beneficial in future research but due to data availability was beyond the scope of the current study.

Not surprisingly, the merchantable volume estimates from forest cover data for blocks with timber cruising data (OR, NWB, FR) were on average closer to harvest scales compared to forest cover estimates derived solely from air photo interpretation. At the Franklin River site, blocks with hemlock as the leading dominant species instead of Douglas-fir also tended to show the largest differences between the harvest scale and the HB merchantable volume results, indicating a possible lack of stability in model transferability as stand species characteristics change. This should be expected as western hemlock and Douglas-fir dominated stands appear similar in point cloud structure despite having slightly different tapers and densities [64,65]. This is also similar to Tompalski et al.'s [27] findings where random forest model predictions of wood volume decreased as the proportions of hemlock and Douglas-fir changed between sites with otherwise similar stand characteristics. This would suggest that if the IT species could be detected, it could improve the HB model.

Comparing the merchantable volume results against the harvest scale showed that the HB model performed better than the forest cover data for this study. The HB model showed that the average absolute difference across OR, NWB, and FR blocks was 14% of the average harvest scale, whereas the average absolute difference was 21% of the harvest scale for the forest cover data. The HB model results from this study are higher than the AB model results reported by White et al. [26], which were on average 6.7% less than the harvest scale. However, the stands examined by White et al. [26] were at a higher elevation and covered a lower overall volume distribution than the coastal forest in this study, which could explain the increased differences between HB merchantable volume and harvest scales.

Comparisons of non-merchantable volume estimates show that HB model results were higher and significantly different from waste and residue survey (WRS) estimates and lower but not significantly different from semi-automated log delineation plus piles estimates (SLDP). Previous research comparing WRS and SLDP methods found that, particularly for the piled and heavy roadside stratum, WRS methods can lead to underestimates of residue volumes depending on sampling intensity [15]. In the OR and NWB sites, the number of WRS sample plots per stratum was much greater than at the FR sites, and thus the differences between the WRS and SLDP methods were lower at these sites (Table 6). In another approach utilizing LiDAR data, Heinaro et al. [66] attempted to segment the LiDAR point cloud to detect coarse woody debris under the canopy. Results from that study indicated that point density and stand characteristics, such as canopy cover, significantly impact the ability to produce accurate ground classifications and resolve the under-canopy structure [66].

For forest managers these pre-harvest HB models allow for wall-to-wall estimation within a harvest block of potential merchantable and non-merchantable wood volumes. In Canadian managed forests, harvesting operations often result in large amounts of residues at the roadside which are piled and burned [15]. The improved pre-harvest estimation of the amount of non-merchantable volumes from HB models would allow forest managers the opportunity to contract the extraction of these residues instead of burning them on site. While this study shows the potential for HB models to be developed and applied utilizing existing spatial and field data, the collection of co-incident LiDAR and imagery from the same sensors over the entire study area has the potential to lessen the amount of uncertainty in model results. Additionally, future applications of the HB methods should

investigate the inclusion of other environmental proxy variables that can be derived from remotely sensed data such as a topographic wetness index.

## 5. Conclusions

The results of this study demonstrate the ability for a hybrid enhanced forest inventory model to be used for pre-harvest estimations of non-merchantable volume that may be left post-harvest as logging residues. Additionally, this study highlighted that individual tree metrics could rank as important predictor metrics when using a Boruta variable selection method. This study also demonstrated the transferability of area-based models to areas with stable and similar point cloud structure, after point thinning, and similar forest structure characteristics. Future work should examine if completing segmentations before point cloud thinning offers any improvements, if the inclusion of other environmental or voxelized predictor metrics offers improved model estimates, and what the impacts of field plot sampling distribution are on estimates of merchantable and non-merchantable wood volumes. With further advancements, a hybrid enhanced forest inventory model could assist with forecasting non-merchantable wood volume available from future harvest blocks for use as bioenergy fuel or bioproducts such as wood pellets. Better forecasting of non-merchantable wood volumes allows for the economic evaluation of extracting these materials before stands are cut and residues burned or started to decompose. Additionally, the methods demonstrated here provide forest managers with the opportunity to analyze block-level harvest efficiencies rapidly.

**Supplementary Materials:** The following supporting information can be downloaded at: <https://www.mdpi.com/article/10.3390/rs14092204/s1>, Table S1: Flight characteristics for post-harvest data collection at Franklin River site. Table S2: Oyster River plot level summaries and LiDAR metrics used in merchantable volume HB model training. Table S3: Victoria Watershed South plot level summaries and LiDAR metrics used in merchantable volume HB model training. Table S4: Victoria Watershed North plot level summaries and LiDAR metrics used in merchantable volume HB model training. Table S5: Oyster River plot level summaries and LiDAR metrics used in non-merchantable volume HB model training. Table S6: Victoria Watershed South plot level summaries and LiDAR metrics used in non-merchantable volume HB model training. Table S7: Victoria Watershed North plot level summaries and LiDAR metrics used in non-merchantable volume HB model training. Table S8: WRS stratum average densities, GIS derived total stratum area, and total volume for FR blocks. Table S9: SLD stratum and block level total volume estimates.

**Author Contributions:** Conceptualization, J.A.T. and J.K.; methodology, J.K. and J.A.T.; formal analysis, J.K.; investigation, J.A.T. and J.K.; data curation, J.K.; writing—original draft preparation, J.K., J.A.T. and C.B.; writing—review and editing, J.K., J.A.T. and C.B.; visualization, J.K.; supervision, C.B. and J.A.T.; project administration, J.A.T. and C.B.; funding acquisition, J.A.T. and C.B. All authors have read and agreed to the published version of the manuscript.

**Funding:** This research was funded by the Forest Innovation Program: Regional Science Supporting the Forest Bioeconomy. The APC was funded by the Canadian Wood Fibre Centre and the University of Victoria SURREAL lab.

**Data Availability Statement:** The data presented in this study are available in the article and Supplementary Materials. Additional data are available on request from the corresponding author.

**Acknowledgments:** Inventory plot measurements at the Sooke Lake watershed were supported by Joel Ussery of Capital Regional District, Canadian Forest Service staff Nicholas Conder, Liane Brooks, Matthew Rempel, and University of Alberta MSc student Kaitlyn Schurmann. Demographic plots at the Sooke Lake watershed had been established by Fangliang He of the University of Alberta, and remeasurements supported by Fangliang He, Joel Ussery of Capital Regional District, Canadian Forest Service staff Nicholas Conder, Liane Brooks, Matthew Rempel, and University of Alberta MSc student Kaitlyn Schurmann. At Oyster River, we thank Timberwest staff, Bill Gurzmacher and Shawn McLennan, Canadian Forest Service staff Nicholas Condor, Robert Ferris, Antonine Lalumiere, Vince Waring, Chantal Lachance and Mihai Voicu and Timberwest consultants Dick Mack, Laura Stanton, and Edith Li for assistance with sample data and preparation. At Northwest Bay, we thank



Island Timberlands staff Steve Mjaaland, Ken Epps, Gavin Cook, Gary Medves and the crew of Contour Forest Consultants Inc, and Canadian Forest Service staff Nicholas Condor, Shannah Beattie, Stephen Gray, and Byron Smiley. Graydon Shevchenko and John Ziemanski of Coastal Resource Mapping conducted RPA flights at Northwest Bay and Franklin River. At Franklin River, we thank Western Forest Products staff Mike Davis, Steve Platt, Erin Badesso, and Francois Warren. We also thank Canadian Forest Service staff Francois Gougeon for continually developing and supporting the semi-automated log delineation algorithms. Funding for this study came from the Forest Innovation Program: Regional Science Supporting the Forest Bioeconomy. We acknowledge the traditional territories of the Huu-ay-aht, T'Sou-ke, Nanoose, and Homalco First Nations, whose relationship with the lands where the research sites for this study were located continues to this day.

**Conflicts of Interest:** The authors declare no conflict of interest.

## References

1. Ninan, K.N.; Inoue, M. Valuing forest ecosystem services: What we know and what we 'don't. *Ecol. Econ.* **2013**, *93*, 137–149. [[CrossRef](#)]
2. Pan, Y.; Birdsey, R.A.; Fang, J.; Houghton, R.; Kauppi, P.E.; Kurz, W.A.; Phillips, O.L.; Shvidenko, A.; Lewis, S.L.; Canadell, J.G.; et al. A large and persistent carbon sink in the world's forests. *Science* **2011**, *333*, 988–993. [[CrossRef](#)] [[PubMed](#)]
3. Natural Resources Canada. *The State of Canada's Forests*; Annual Report 2019; Natural Resources Canada, Canadian Forest Service: Ottawa, ON, Canada, 2020; p. 88. Available online: [https://cfs.nrcan.gc.ca/publications?id=40219&lang=en\\_CA](https://cfs.nrcan.gc.ca/publications?id=40219&lang=en_CA) (accessed on 15 October 2020).
4. Nabuurs, G.J.; Masera, O.; Andrasko, K.; Benitez-Ponce, P.; Boer, R.; Dutschke, M.; Elsiddig, E.; Ford-Robertson, J.; Frumhoff, P.; Karjalainen, T.; et al. Chapter 9: Forestry. In *Climate Change 2007: Mitigation*; Cambridge University Press: Cambridge, UK; New York, NY, USA, 2007.
5. Trofymow, J.A.; Stinson, G.; Kurz, W.A. Derivation of a spatially explicit 86-year retrospective carbon budget for a landscape undergoing conversion from old-growth to managed forests on Vancouver Island, BC. *Forest Ecol. Manag.* **2008**, *256*, 1677–1691. [[CrossRef](#)]
6. Cambero, C.; Sowlati, T.; Marinescu, M.; Röser, D. Strategic optimization of forest residues to bioenergy and biofuel supply chain. *Int. J. Energy Res.* **2015**, *39*, 439–452. [[CrossRef](#)]
7. Smyth, C.E.; Stinson, G.; Neilson, E.; Lemprière, T.C.; Hafer, M.; Rampley, G.J.; Kurz, W.A. Quantifying the biophysical climate change mitigation potential of Canada's forest sector. *Biogeosciences* **2014**, *11*, 3515–3529. [[CrossRef](#)]
8. Xu, Z.; Smyth, C.E.; Lemprière, T.C.; Rampley, G.J.; Kurz, W.A. Climate change mitigation strategies in the forest sector: Biophysical impacts and economic implications in British Columbia, Canada. *Mitig. Adapt. Strateg. Glob. Change* **2018**, *23*, 257–290. [[CrossRef](#)]
9. Marland, G.; Pielke, R.A.; Apps, M.; Avissar, R.; Betts, R.A.; Davis, K.J.; Frumhoff, P.C.; Jackson, S.T.; Joyce, L.A.; Kauppi, P.; et al. The climatic impacts of land surface change and carbon management, and the implications for climate-change mitigation policy. *Clim. Policy* **2003**, *3*, 149–157. [[CrossRef](#)]
10. Pacala, S.; Socolow, R. Stabilization wedges: Solving the climate problem for the next 50 years with current technologies. *Science* **2004**, *305*, 968–972. [[CrossRef](#)]
11. IPCC. *2014 Revised Supplementary Methods and Good Practice Guidance Arising from the Kyoto Protocol*; Hiraiishi, T., Krug, T., Tanabe, K., Srivastava, N., Baasansuren, J., Fukuda, M., Troxler, T.G., Eds.; IPCC: Geneva, Switzerland, 2013.
12. Barrette, J.; Paré, D.; Manka, F.; Guindon, L.; Bernier, P.; Titus, B. Forecasting the spatial distribution of logging residues across the Canadian managed forest. *Can. J. For. Res.* **2018**, *48*, 1470–1481. [[CrossRef](#)]
13. Dymond, C.C.; Kamp, A. Fibre use, net calorific value, and consumption of forest-derived bioenergy in British Columbia, Canada. *Biomass Bioenergy* **2014**, *70*, 217–224. [[CrossRef](#)]
14. Smyth, C.; Rampley, G.; Lemprière, T.C.; Schwab, O.; Kurz, W.A. Estimating product and energy substitution benefits in national-scale mitigation analyses for Canada. *Glob. Change Biol. Bioenergy* **2017**, *9*, 1071–1084. [[CrossRef](#)]
15. Trofymow, J.A.; Coops, N.C.; Hayhurst, D. Comparison of remote sensing and ground-based methods for determining residue burn pile wood volumes and biomass. *Can. J. For. Res.* **2014**, *44*, 182–194. [[CrossRef](#)]
16. Titus, B.D.; Brown, K.; Helmisaari, H.S.; Vanguelova, E.; Stupak, I.; Evans, A.; Clarke, N.; Guidi, C.; Bruckman, V.J.; Varnagiryte-Kabasinskiene, I.; et al. Sustainable forest biomass: A review of current residue harvesting guidelines. *Energy Sustain. Soc.* **2021**, *11*, 10. [[CrossRef](#)]
17. Dymond, C.C.; Titus, B.D.; Stinson, G.; Kurz, W.A. Future quantities and spatial distribution of harvesting residue and dead wood from natural disturbances in Canada. *For. Ecol. Manag.* **2010**, *260*, 181–192. [[CrossRef](#)]
18. Wells, L.A.; Chung, W.; Anderson, N.M.; Hogland, J.S. Spatial and temporal quantification of forest residue volumes and delivered costs. *Can. J. For. Res.* **2016**, *46*, 832–843. [[CrossRef](#)]
19. Pokharel, R.; Grala, R.K.; Latta, G.S.; Grebner, D.L.; Grado, S.C.; Poudel, J. Availability of logging residues and likelihood of their utilization for electricity production in the US south. *J. For.* **2019**, *117*, 543–559. [[CrossRef](#)]

20. Ranta, T. Logging residues from regeneration fellings for biofuel production—A GIS-based availability analysis in Finland. *Biomass Bioenergy* **2005**, *28*, 171–182. [[CrossRef](#)]
21. Mansuy, N.; Paré, D.; Thiffault, E.; Bernier, P.Y.; Cyr, G.; Manka, F.; Lafleur, B.; Guindon, L. Estimating the spatial distribution and locating hotspots of forest biomass from harvest residues and fire-damaged stands in Canada's managed forests. *Biomass Bioenergy* **2017**, *97*, 90–99. [[CrossRef](#)]
22. Sidders, D.; Joss, B.; Keddy, T. *Project TID8 25B: GIS-Based Inventory and Analysis of Forestry and Agriculture Biomass*; Natural Resources Canada: Ottawa, ON, Canada, 2008.
23. Ferster, C.J.; Coops, N.C.; Trofymow, J.A.T. Aboveground large tree mass estimation in a coastal forest in British Columbia using plot-level metrics and individual tree detection from lidar. *Can. J. Remote Sens.* **2009**, *35*, 270–275. [[CrossRef](#)]
24. Næsset, E. Predicting forest stand characteristics with airborne scanning laser using a practical two-stage procedure and field data. *Remote Sens. Environ.* **2002**, *80*, 88–99. [[CrossRef](#)]
25. Woods, M.; Lim, K.; Treitz, P. Predicting forest stand variables from LiDAR data in the Great Lakes—St. Lawrence forest of Ontario. *For. Chron.* **2008**, *84*, 827–839. [[CrossRef](#)]
26. White, J.C.; Wulder, M.A.; Buckmaster, G. Validating estimates of merchantable volume from airborne laser scanning (ALS) data using weight scale data. *For. Chron.* **2014**, *90*, 378–385. [[CrossRef](#)]
27. Tompalski, P.; White, J.C.; Coops, N.C.; Wulder, M.A. Demonstrating the transferability of forest inventory attribute models derived using airborne laser scanning data. *Remote Sens. Environ.* **2019**, *227*, 110–124. [[CrossRef](#)]
28. Kelley, J.; Trofymow, J.A.; Metsaranta, J.M.; Filipescu, C.N.; Bone, C. Use of multi-temporal LiDAR to quantify fertilization effects on stand volume and biomass in late-rotation coastal Douglas-fir forests. *Forests* **2021**, *12*, 517. [[CrossRef](#)]
29. White, J.C.; Wulder, M.A.; Varhola, A.; Vastaranta, M.; Coops, N.C.; Cook, B.D.; Pitt, D.; Woods, M. *A Best Practices Guide for Generating Forest Inventory Attributes from Airborne Laser Scanning Data Using an Area-Based Approach*; Information Report FI-X-010; Natural Resources Canada: Victoria, BC, Canada, 2013; p. 39. Available online: <https://cfs.nrcan.gc.ca/publications?id=34887> (accessed on 16 January 2018).
30. Holopainen, M.; Vastaranta, M.; Rasinmäki, J.; Kalliovirta, J.; Mäkinen, A.; Haapanen, R.; Melkas, T.; Yu, X.; Hyyppä, J. Uncertainty in timber assortment estimates predicted from forest inventory data. *Eur. J. For. Res.* **2010**, *129*, 1131–1142. [[CrossRef](#)]
31. Korhonen, L.; Peuhkurinen, J.; Malinen, J.; Suvanto, A.; Maltamo, M.; Packalen, P.; Kangas, J. The use of airborne laser scanning to estimate sawlog volumes. *For. Int. J. For. Res.* **2008**, *81*, 499–510.
32. Gougeon, F.A.; Leckie, D.G. *Pacific Forestry Centre. Forest Information Extraction from High Spatial Resolution Images Using an Individual Tree Crown Approach*; Natural Resources Canada: Victoria, BC, Canada, 2003.
33. Dalponte, M.; Coomes, D.A. Tree-centric mapping of forest carbon density from airborne laser scanning and hyperspectral data. *Methods Ecol. Evol.* **2016**, *7*, 1236–1245. [[CrossRef](#)]
34. Li, W.; Guo, Q.; Jakubowski, M.K.; Kelly, M. A new method for segmenting individual trees from the Lidar point cloud. *Photogramm. Eng. Remote Sens.* **2012**, *78*, 75–84. [[CrossRef](#)]
35. Jucker, T.; Caspersen, J.; Chave, J.; Antin, C.; Barbier, N.; Bongers, F.; Dalponte, M.; van Ewijk, K.Y.; Forrester, D.I.; Haeni, M.; et al. Allometric equations for integrating remote sensing imagery into forest monitoring programmes. *Glob. Change Biol.* **2017**, *23*, 177–190. [[CrossRef](#)]
36. Kozak, A. Development of Taper Equations by BEC Zones and Species. Available online: <https://www.for.gov.bc.ca/hfd/library/documents/bib95354a.pdf> (accessed on 20 October 2018).
37. Blackburn, R.C.; Buscaglia, R.; Sanchez Meador, A. Mixtures of airborne lidar-based approaches improve predictions of forest structure. *Can. J. For. Res.* **2021**, *51*, 1106–1116. [[CrossRef](#)]
38. Hyyppä, J.; Yu, X.; Hyyppä, H.; Vastaranta, M.; Holopainen, M.; Kukko, A.; Kaartinen, H.; Jaakkola, A.; Vaaja, M.; Koskinen, J.; et al. Advances in forest inventory using airborne laser scanning. *Remote Sens.* **2012**, *4*, 1190–1207. [[CrossRef](#)]
39. Kankare, V.; Vastaranta, M.; Holopainen, M.; Rätty, M.; Yu, X.; Hyyppä, J.; Hyyppä, H.; Alho, P.; Viitala, R. Retrieval of forest aboveground biomass and stem volume with airborne scanning LiDAR. *Remote Sens.* **2013**, *5*, 2257–2274. [[CrossRef](#)]
40. Trofymow, J.A.; Kelley, J.; Gougeon, F. Comparison of geospatial and ground-based methods for determining post-harvest dispersed woody residues. *Can. J. For. Res.* **2019**, *49*, 1277–1288. [[CrossRef](#)]
41. Trofymow, J.A.; Gougeon, F.; Kelley, J. *Determination of Dispersed and Piled Post-Harvest Residues in Coastal Douglas-Fir Cutblocks Using Unmanned Aerial Vehicle Imagery and Ground-Based Surveys*; Information Report FI-X-015; Natural Resources Canada: Victoria, BC, Canada, 2017; p. 39. Available online: <http://cfs.nrcan.gc.ca/publications?id=38836> (accessed on 11 July 2019).
42. Pojar, J.; Klinka, K.; Demarchi, D.A. Chapter 6: Coastal Western Hemlock Zone. In *Ecosystems of British Columbia*; BC Special Report Series No., 6; Meidinger, D., Pojar, J., Eds.; BC Ministry of Forests: Victoria, BC, Canada, 1991; pp. 95–111.
43. Coursolle, C.; Margolis, H.A.; Giasson, M.; Bernier, P.; Amiro, B.D.; Arain, M.A.; Barr, A.G.; Black, T.A.; Goulden, M.L.; McCaughey, J.H. Influence of stand age on the magnitude and seasonality of carbon fluxes in Canadian forests. *Agric. For. Meteorol.* **2012**, *165*, 136–148. [[CrossRef](#)]
44. Trofymow, J.A.; Porter, G.L.; Blackwell, B.A.; Marshall, V.; Arskey, R.; Pollard, D. *Chronosequences Selected for Research into the Effects of Converting Coastal British Columbia Old Growth Forests to Managed Forests: An Establishment Report*; Information Report BC-X-374; Pacific Forestry Centre: Victoria, BC, Canada, 1997; p. 137.
45. Blackwell, B.A.; Trofymow, J.A.; Hedberg, H.A. *Pacific Forestry Centre. Stand Structure and Species Composition in Chronosequences of Forests on Southern Vancouver Island*; Natural Resources Canada: Victoria, BC, Canada, 2002.

46. He, F.; Duncan, R.P. Density-dependent effects on tree survival in an old-growth Douglas fir forest. *J. Ecol.* **2000**, *88*, 676–688. [[CrossRef](#)]
47. Hilker, T.; van Leeuwen, M.; Coops, N.C.; Wulder, M.A.; Newnham, G.J.; Jupp, D.L.B.; Culvenor, D.S. Comparing canopy metrics derived from terrestrial and airborne laser scanning in a douglas-fir dominated forest stand. *Trees* **2010**, *24*, 819–832. [[CrossRef](#)]
48. Quinn, G.S. Derivation of Forest Productivity and Structure Attributes from Remote Sensing Imaging Technology. Ph.D. Thesis, University of Victoria, Victoria, BC, Canada, 2018. Available online: <https://dspace.library.uvic.ca:8443/handle/1828/10471> (accessed on 27 March 2022).
49. Roussel, J.; Auty, D.; Coops, N.C.; Tompalski, P.; Goodbody, T.R.; Meador, A.S.; Achim, A. LidR: An R package for analysis of airborne laser scanning (ALS) data. *Remote Sens. Environ.* **2020**, *251*, 112061. [[CrossRef](#)]
50. Khosravipour, A.; Skidmore, A.K.; Isenburg, M.; Wang, T.; Hussin, Y.A. Generating pit-free canopy height models from airborne Lidar. *Photogramm. Eng. Remote Sens.* **2014**, *80*, 863–872. [[CrossRef](#)]
51. National Forest Inventory. *Canada's National Forest Inventory Ground Sampling Guidelines: Specifications for Ongoing Measurements*; Version 5.0; National Forest Inventory: Farnham, UK, 2008. Available online: [https://nfi.nfis.org/resources/groundplot/Gp\\_guidelines\\_v5.0.pdf](https://nfi.nfis.org/resources/groundplot/Gp_guidelines_v5.0.pdf) (accessed on 15 August 2020).
52. Timber Pricing Branch. *Scaling Manual*; Ministry of Forests Lands and Natural Resource Operations: Victoria, BC, Canada, 2011. Available online: <https://www.for.gov.bc.ca/ftp/hva/external/!publish/web/manuals/Scaling/2011/Scaling2011NovMaster.pdf> (accessed on 27 March 2022).
53. Kurska, M.B.; Rudnicki, W.R. Feature selection with the Boruta package. *J. Stat. Softw.* **2010**, *36*, 1–13. [[CrossRef](#)]
54. Kuhn, M. Building predictive models in R using the caret package. *J. Stat. Softw.* **2008**, *28*, 1–26. [[CrossRef](#)]
55. Liaw, A.; Wiener, M. Classification and regression by random forest. *R News* **2002**, *2*, 18–22.
56. White, J.C.; Stepper, C.; Tompalski, P.; Coops, N.C.; Wulder, M.A. Comparing ALS and image-based point cloud metrics and modelled forest inventory attributes in a complex coastal forest environment. *Forests* **2015**, *6*, 3704–3732. [[CrossRef](#)]
57. Metsaranta, J.M.; Trofymow, J.A.; Black, T.A.; Jassal, R.S. Long-term time series of annual ecosystem production (1985–2010) derived from tree rings in Douglas-fir stands on Vancouver Island, Canada using a hybrid biometric-modelling approach. *For. Ecol. Manag.* **2018**, *429*, 57–68. [[CrossRef](#)]
58. Province of British Columbia. Forest Inventory. Available online: <https://www2.gov.bc.ca/gov/content/industry/forestry/managing-our-forest-resources/forest-inventory> (accessed on 29 May 2021).
59. Province of British Columbia. Provincial Logging Residue and Waste Measurement Procedures Manual. Available online: [https://www2.gov.bc.ca/assets/gov/farming-natural-resources-and-industry/forestry/timber-pricing/residue-and-waste/rwp\\_amend\\_28.pdf](https://www2.gov.bc.ca/assets/gov/farming-natural-resources-and-industry/forestry/timber-pricing/residue-and-waste/rwp_amend_28.pdf) (accessed on 29 May 2021).
60. Shapiro, S.S.; Wilk, M.B. An analysis of variance test for normality (complete samples). *Biometrika* **1965**, *52*, 591–611. [[CrossRef](#)]
61. Latifi, H.; Nothdurft, A.; Koch, B. Non-parametric prediction and mapping of standing timber volume and biomass in a temperate forest: Application of multiple optical/LiDAR-derived predictors. *Forestry* **2010**, *83*, 395–407. [[CrossRef](#)]
62. Vastaranta, M.; Wulder, M.A.; White, J.C.; Pekkarinen, A.; Tuominen, S.; Ginzler, C.; Kankare, V.; Holopainen, M.; Hyyppä, J.; Hyyppä, H. Airborne laser scanning and digital stereo imagery measures of forest structure: Comparative results and implications to forest mapping and inventory update. *Can. J. Remote Sens.* **2013**, *39*, 382–395. [[CrossRef](#)]
63. Kotivuori, E.; Korhonen, L.; Packalen, P. Nationwide airborne laser scanning based models for volume, biomass and dominant height in Finland. *Silva Fenn.* **2016**, *50*, 1567. [[CrossRef](#)]
64. Poudel, K.P.; Temesgen, H.; Gray, A.N. Estimating upper stem diameters and volume of Douglas-fir and western hemlock trees in the Pacific Northwest. *For. Ecosyst.* **2018**, *5*, 16. [[CrossRef](#)]
65. Miles, P.D.; Smith, W.B. *Specific Gravity and Other Properties of Wood and Bark for 156 Tree Species Found in North America*; Research Note NRS-38; USDA Forest Service, Northern Research Station: Newtown Square, PA, USA, 2009.
66. Heinaro, E.; Tanhuanpää, T.; Yrttimaa, T.; Holopainen, M.; Vastaranta, M. Airborne laser scanning reveals large tree trunks on forest floor. *For. Ecol. Manag.* **2021**, *491*, 119225. [[CrossRef](#)]